Rev.Adv.Mater.Sci. 6 (2004) 120-130

DEFORMATION-INDUCED SYNTHESIS OF Al-BASED HETEROGENEOUS NANOSCALE MICROSTRUCTURES

R.J. Hebert

Forschungszentrum Karlsruhe GmbH, Institut für Nanotechnologie, P.O. Box 3640, D-76021 Karlsruhe, Germany

Received: March 05, 2004

Abstract. Intense plastic deformation of Al-based crystalline multilayers and amorphous ribbons serves as a processing technique to synthesize nanoscale heterogeneous microstructures with improved mechanical properties. Underlying principles of deformation-induced structural transformations are examined including the strong increase in transformation site densities during deformation and the athermal nature of the structural transformations that should be relevant for a wider class of driven system processing techniques.

1. INTRODUCTION

The development of light-weight, high-strength materials is one of the most abiding and important objectives in materials science. The basis of light-weight, high-strength materials in the field of metallurgical engineering for near ambient temperature applications have been and continue to be mainly Al-based alloys. Magnesium-alloys, titanium-alloys, and polymer composites are alternative light-weight materials with moderate to high-strength at near ambient temperatures, but the comparatively low price combined with an extensive processing experience has certainly enhanced the widespread use of Al-alloys. Progress in the development of structural, light-weight materials was made for many years mainly in the areas of alloy selection, casting and heat treatment. Seminal achievements in the research of strengthening mechanisms such as precipitation strengthening [1,2] were closely related to the ever more demanding mechanical property requirements for structural light-weight alloys.

In recent years, the progress in the development of structural materials has been increasingly biased by concepts akin to nanoscale materials. Two concepts have received particular attention: improvements based on size-scale effects, i.e. property changes that occur as a result of the reduction of a characteristic size scale to the nanometer level [3], and novel materials properties that emerge from high volume fractions or specific interface areas of nanometer-sized phases [4]. An example of size-scale effects that is appealing for structural applications is, for example, the strenghtening effect that is based on an inverse power-law dependence of the strength on a characteristic microstructural length scale [5,6]. Ultrafine-grained materials as well as multilayers with nanoscale layer thicknesses are examples where exceptional strength levels have been achieved due to the refinement of the microstructure to the nanometer scale [7,8].

Aside from size-scale effects, materials with novel properties have emerged because of extremely high specific interface areas in heterogeneous microstructures. Two examples of heterogeneous nanoscale microstructures are highlighted in this article. Based on a repeated rolling and folding process of elemental foils, sheet materials can be processed at true

Corresponding author: R.J. Hebert, e-mail: rainer.hebert@int.fzk.de

strain levels in excess of ten. Similar to related severe plastic deformation techniques such as equal channel angular extrusion, bulk samples are retained during the rolling and folding process while refining the microstructure to a nanometer-level [9-12]. For the sustained rolling and folding deformation of multilayers comprised of dissimilar elemental foils, mixing reactions can be induced in addition to the reduction in layer thickness that offer the opportunity to synthesize novel phases [10, 13]. Al-Y and Al-Y-Fe multilayers serve in this article as model systems to highlight key aspects of cold-rolling induced amorphization reactions. The analysis of the cold-rolling experiments follows two main schemes, the change of the layer arrangement with folding and rolling, and the mixing reactions at the interfaces.

The intense deformation of multilayers involves a multitude of complex phenomena, for example, the microstructure evolution within each of the layers or the evolution and the effect of residual stresses on the structural transformations. In this work, however, the emphasis is placed on the effect of repeated folding and rolling on the structural transformations and on the identification of transformation principles that apply not only to deformation-induced mixing and amorphization reactions, but could be applied to similar deformation processes involving a repetitive forcing of heterogeneous microstructures.

An entirely different approach to the advancement of Al-alloys emerged with the discovery of Al-based metallic glasses by Inoue and coworkers at Tohoku University [14] and independently by Shiflet and coworkers at the University of Virginia in 1988 [15]. The transition from crystalline materials to amorphous phases propelled the amorphous Al-alloys to a new strength/density domain that had previously been limited to ceramic materials [16]. Soon after the discovery of Al-glasses, it was found that the strength could be enhanced further with the controlled primary crystallization of nanometer-sized Al-crystals embedded in the amorphous matrix. Careful annealing experiments yielded amorphous materials with particle densities of up to 10^{23} m^{-3} [17,18]. While the annealing-induced crystallization processes are subject to ongoing investigations [19,20], deformation experiments with melt-spun ribbons and bulk metallic glasses have revealed that nanocrystallites can also be induced during bending, cold-rolling, or nanoindentation of metallic glasses at near-ambient temperatures [21-25]. Based on rolling and on annealing experiments mainly with melt-spun amorphous $Al_{88}Y_7Fe_5$ ribbons, distinctions are highlighted between thermally-induced and deformation-induced crystallization reactions. Moreover, the deformation-induced crystallization reactions are compared with the mixing reactions in multilayers in order to identify common underlying grounds.

2. EXPERIMENTAL

For the rolling of the multilayers, arrays of elemental foils were stacked with the desired nominal composition, wound manually as a spiral, and then rolled and folded repeatedly in a two-high rolling mill. Details of the rolling and folding process are given in [26]. Due to the folding process, the sample maintains a thickness of approximately 100 micrometers. The true strain was determined from measurements of the sample thickness before rolling, t_i, and after rolling, t_f, and is given as ln (t_i/t_f). The rolling and folding process allows for the processing of samples with a true strain in excess of -10.

Amorphous ribbons were melt-spun in a single-roller melt-spinner at a wheel-speed of 42 m/s in a Helium atmosphere of 200 mbar pressure. The ribbon lengths used for the experiments was approximately 1 m with a width of 4 mm and a thickness of approximately 30 μm. The melt-spun ribbons were rolled and folded as described in [26]. Prior to the rolling, each ribbon piece was examined based on X-ray diffraction in order to ensure that all ribbon pieces were initially X-ray amorphous. Moreover, the continuous heating differential scanning calorimetry (DSC) curves of pieces from both ends of the ribbons were examined and found to be identical. This precaution is necessary since the thermal behavior and the concentration of clusters in the amorphous matrix in ribbons with the same composition can change slightly from batch to batch and also along the ribbon. For the X-ray diffraction (XRD) analysis, Philips X'Pert and a STOE diffractometer were used with Cu-K_α radiation. The scanning electron microscopy (SEM) analysis was conducted with a JEOL-6100 SEM and the transmission electron microscopy (TEM) analysis with a Philips CM30 TEM (accelerating voltage: 300 kV). The rolled ribbons were electrolytically thinned with a mixture of nitric acid (1/3 volume fraction) and methanol (2/3 volume fraction). Comparing the images at the beginning and at the end of the TEM analysis of a particular sample area, it could be ruled out that the electron beam induced nanocrystallites during the TEM investigations. In order to observe all nanocrystallites in a given viewing area, particular the nanocrystals in

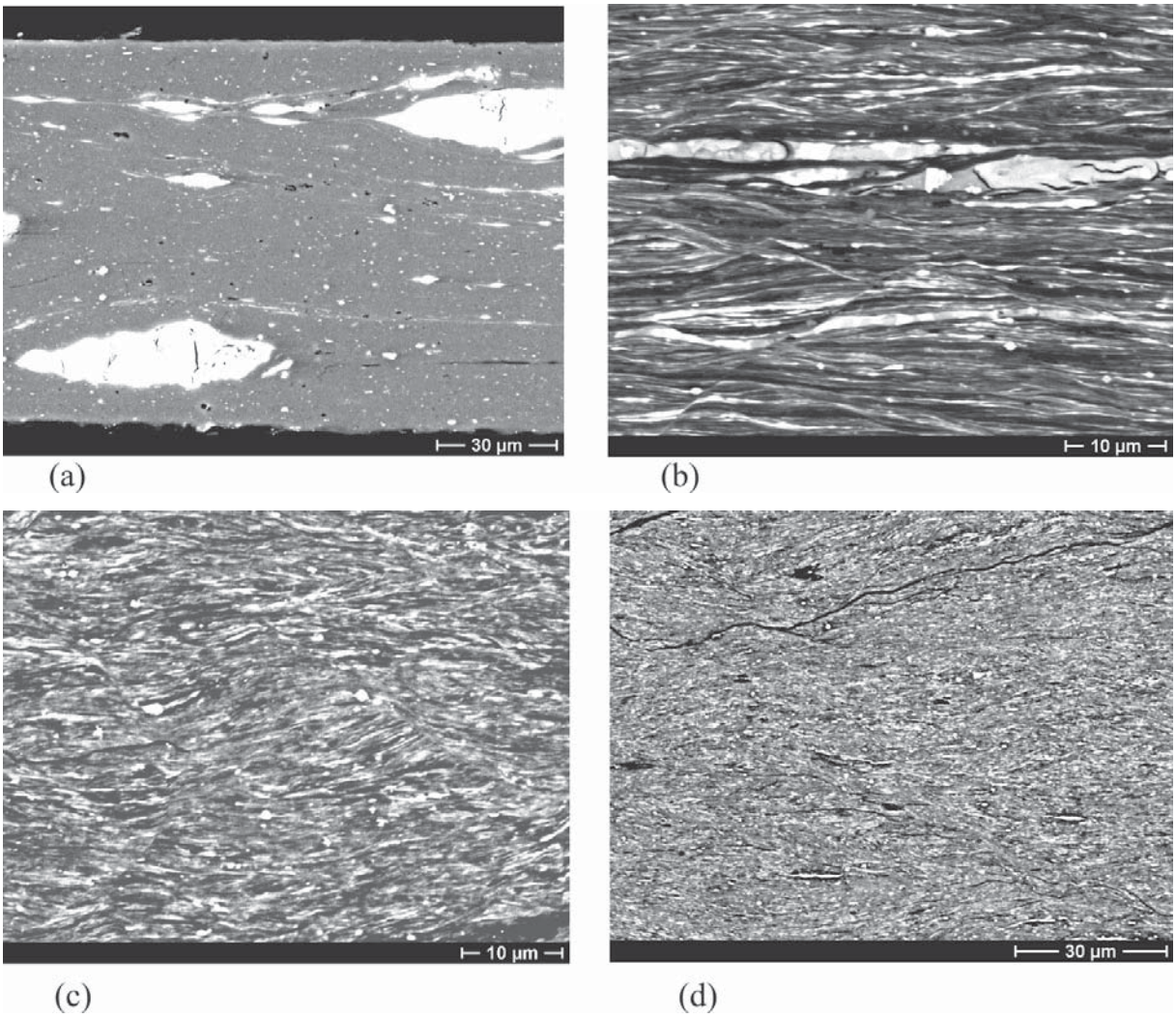

Fig.1. Cross-sectional SEM images of an $Al_{89}Y_{11}$ multilayer. (a) ε_{true} = -13, (b) ε_{true} = -31, (c) ε_{true} = -50, (d) ε_{true} = -70.

shear bands, some dark-field images were taken in a dynamic hollow cone mode, i.e. with the broad halo in the electron diffraction pattern centered on the optical axis and rotating continuously. Since the exposure time for the images was approximately three times the time for one rotation of the halo, all nanocrystallites that existed in the TEM viewing volumes were visible in the images. The calorimetric analysis was conducted with a Perkin Elmer Pyris DSC1 and a standard heating rate of 20 K/min.

3. RESULTS AND DISCUSSION

3.1. Rolling of Al-Y and Al-Y-Fe multilayers

Layer refinement. A sequence of cross-sectional SEM images of a cold-rolled multilayer with a nominal composition of $Al_{89}Y_{11}$ is depicted in Fig. 1. The bright layers in the images correspond to Y. The initial foil thickness of the Y and Al foils was 25 micrometers. The image depicted in Fig. 1a shows that the Y layers have disintegrated into pieces with a thickness that ranges from nearly 25 micrometers to less than one micrometer. The original layers have ruptured into pieces that often display a cigar-shaped cross-sectional morphology. Inside the

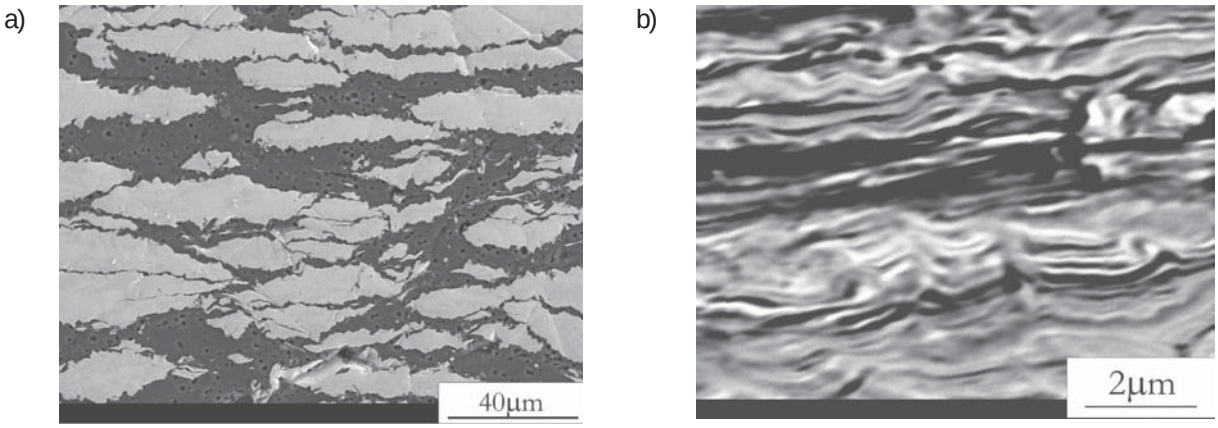

Fig. 2. (a) Cross-sectional SEM image of an Al-Ta multilayer at ε_{true} = -10, (b) Cross-sectional SEM image of an $Mo_{55}Ta_{45}$ multilayer at ε_{true} = -20.

original layers, cracks are visible that can extend to the Al/Y interface where Y pieces can detach from the original Y layers. As a result of the detachment process, Y pieces with a thickness of less than 1 micrometer are dispersed in the Al matrix. In addition to the small Y particles, elongated Y layers form at the tip of the original layers. Figs. 1c and 1d show that with increasing strain the thickness of the Y layers decreases from 25 micrometers initially to less than one micrometer at a strain of -70. While for the Y layers embedded in the Al matrix secondary particles rupture from the original layers at the Al/Y interfaces and develop into secondary layers, the generation of secondary layers at the interfaces of rolled ductile multilayers can also result from an interface roughness. Interface undulations can develop into protrusions into the matrix that become elongated with further deformation [27]. As explained in more detail in [28], for fcc-fcc layer combinations the prediction whether the layers co-deform or rupture into pieces at early deformation stages can be based on the difference in the flow stresses or yield strength between adjacent layers. Since it is the difference between the flow stresses and not the absolute value that is crucial for the layer refinement, elemental layers such as Pt layers can reveal strong differences in the layer cross-section morphology depending on the matrix they are embedded in [29]. The reason why the difference in the yield strength between adjacent layers affects the layer refinement is likely to be related to the interface stress that appears as a result of the yield strength difference when the multilayer is compressed [30]. The layer with the higher flow stress experiences according to [30] a tensile stress at the interface while the softer layer experiences a compressive stress. It must be considered, however, that during the severe deformation of multilayers additional stresses can develop at the interfaces that result, for example, from solubility extensions or from lattice mismatch that can influence the prediction based only on the flow stress differences. If the ratio of the flow stress exceeds a limit that has been found empirically to be approximately three, the matrix can flow past the harder phase [31]. In this case, the harder phase remains nearly undeformed in the matrix and the strain partitions to the matrix. Rolling experiments with Al-Ta showed, for example, that the Ta layers barely refine and even at true strain levels of -10 the Ta layers remained close to their original foil thickness of 25 micrometers as depicted in Fig. 2a. By contrast, rolling of a Mo-Ta multilayer resulted in a co-deformation of both elemental layers (Fig. 2b).

For multilayer systems with three or more components, the strain partitioning can cause the two components that deform in the softer matrix to deform at different rates. An example is shown in Fig. 3 for a multilayer with a nominal composition of $Al_{85}Y_{7.5}Fe_{7.5}$. In the starting multilayer the sequence of the foils was Al/Y/Fe. Fig. 3a reveals that at the early deformation stage the Y and Fe foils remained in contact and in some cases even deformed as a 'bilayer' particle. With increasing strain, however, the Y and Fe layers detached. Since deformation-induced mixing distances across the interfaces are of the order of nanometers [32], in order to generate a ternary mixture, it is necessary that both solute layers in a ternary multilayer are within a distance of the order of nanometers. Clearly, for the $Al_{85}Y_{7.5}Fe_{7.5}$ multilayer depicted in Fig. 3b, the distance between the Fe and the Y layers in the Al

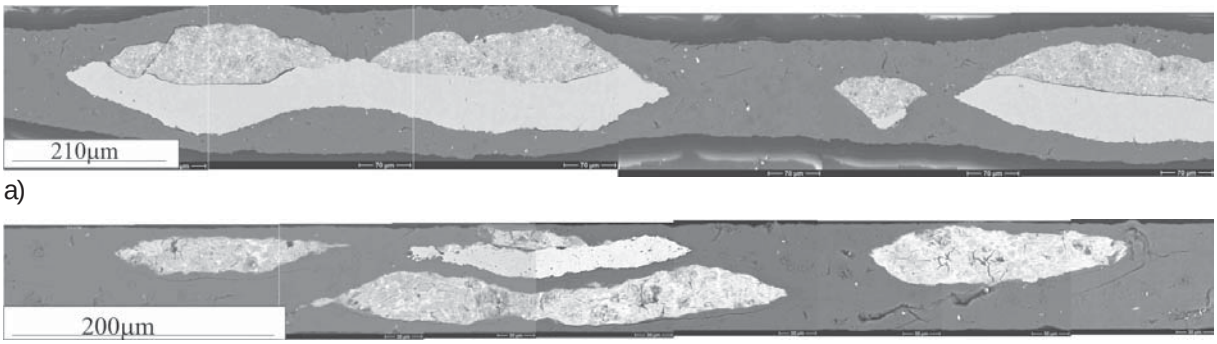

Fig. 3. Cross-sectional SEM images of an $Al_{85}Y_{7.5}Fe_{7.5}$ multilayer at (a) ε_{true} = -1, (b) ε_{true} = -3.

matrix exceeded the nanometer range by far. While in standard rolling operations the distance between layers can not be changed considerably, the combined process of folding and rolling not only enhances the specific interface area, S_V, but also reduces the distance between the layers greatly. The average distance between the Y layers in Fig. 1c, for example, has diminished to a few hundred nanometers from 25 micrometers, initially.

The deformation process has so far been gauged in terms of the overall true strain imparted on the multilayer. For multilayers with strong strain partitioning, the deformation is limited mainly to the matrix and as a consequence the specific interface area does not increase proportionally to the true strain. It has therefore been proposed to use the specific interface area directly as a measure of the multilayer deformation level [28]. A hallmark of the repeated rolling and folding process of multilayers is indeed the strong increase in S_V. Scaled by S_V at the beginning of the deformation process, the relative specific interface area can increase from one to about 8000 as demonstrated for Al-Pt multilayers [28].

Intermixing at interfaces. The effect of the repeated rolling and folding on the $Al_{95}Y_5$ and $Al_{89}Y_{11}$ multilayer, measured based on X-ray diffraction measurements, is depicted in Fig. 4 for both multilayers at a strain of -70. The X-ray patterns show that intermetallic phases have not formed during the rolling up to a strain of -70. However, a broad peak develops in addition to the remaining Al-peaks. Both, the Al-peaks and the Y-peaks shift in position with increasing strain. For the $Al_{95}Y_5$ multilayer, the Al lattice parameter decreases from 4.0450 ± 0.004 Å at a strain of -11 to 4.035 ± 0.012 Å at a strain of -70. The Y lattice parameters change from 3.665 Å (a-axis) at a strain of -11 to 3.644 Å at a strain of -70 and from 5.722 Å (c-axis) at a strain of -11 to 5.728 Å at a strain of -70. The broad peak in the X-ray diffraction pattern can be explained based on the formation of an amorphous phase. Although the nominal multilayer composition of $Al_{95}Y_5$ is outside the reported glass-forming range for the Al-Y system, the local composition in the mixing zone at the interfaces can be within the glass forming range as long as the remaining crystalline phases comply with the mass balance.

For the $Al_{89}Y_{11}$ sample, at a strain of -70 the intensity of the Y peaks has vanished. This is surprising given that at the same strain the $Al_{95}Y_5$ sample did reveal Y peaks and the Y foils used for the two rolling experiments had initially the same thickness. The unexpected behavior might be linked to the dependence of the strain partitioning on the ratio of the layer thickness to the average distance between the layers. A relation between the distance between inclusions and their aspect ratio has been established in structural geology. The model proposed in [33] assumes a matrix with Newtonian viscous behavior and concludes that the larger the concentration of inclusions in the matrix, the larger is the ratio of the flattening rates between the stiff inclusions and the matrix, i.e., the strain partitioning. Following this argument, the strain partitioning would be more pronounced in the $Al_{89}Y_{11}$ sample. Although the model proposed in [33] has yet to be verified experimentally for metallic multilayers, the relative motion of adjacent layers at the interfaces during deformation that scales with the level of strain partitioning can be expected to be crucial for the mechanism of the intermixing reactions. While dislocations play an important role in existing models of intermixing reactions [34] across interfaces, molecu-

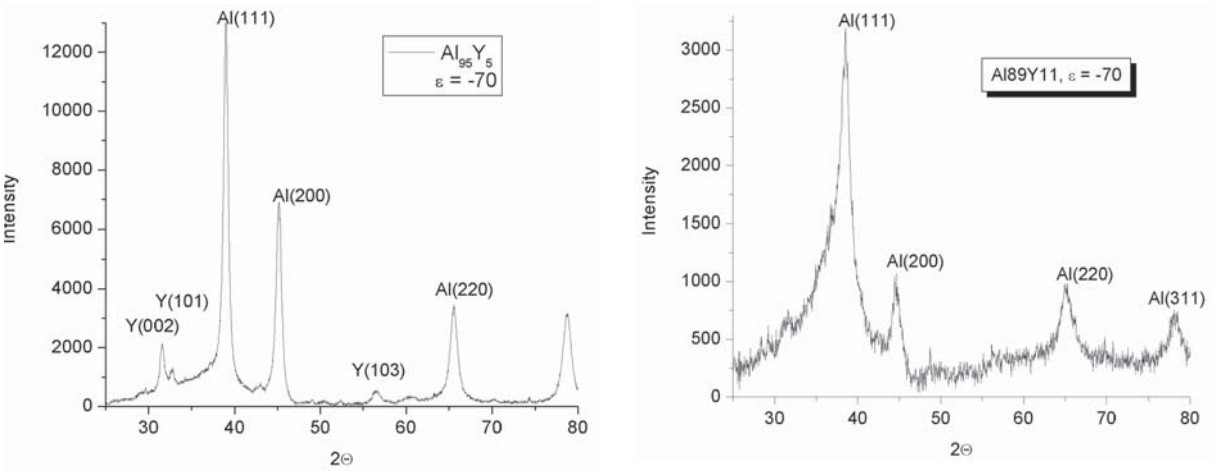

Fig. 4. XRD patterns of an $Al_{95}Y_5$ multilayer (a) and an $Al_{89}Y_{11}$ multilayer, both at ε_{true} = -70.

lar dynamic simulations have revealed that the mixing should be attributed to an interface roughening effect [35].

Amorphization criteria for cold-rolling. The insight into the layer refinement behavior of multilayers during deformation together with phase diagram information and the results obtained with respect to the alloying behavior at interfaces allow to draw conclusions about the amorphization criteria for cold-rolling. From a thermodynamic viewpoint, mixing reactions are observed to occur more rapidly as a function of strain for systems with a strong negative heat of mixing. However, multilayer systems with a heat of mixing in excess of approximately -60 kJ/mol between the elemental foils such as Al-Pt or Al-Pd often react exothermically to form intermetallic phases during rolling. On the other hand, intermixing of layers with a heat of mixing near zero, for example the Al-Cu system, remains very limited even after continued rolling and even if the increase in the relative specific interface area at true strain levels of 40 or more is of the order of 10^3 as it is the case for the Al-Cu multilayer. The layer refinement to a layer thickness at the nanometer scale is therefore a necessary but not a sufficient condition and must be combined with the requirement of a negative heat of mixing in order to obtain significant volume fractions of amorphous phase.

3.2. Cold-rolling of melt-spun amorphous ribbons

In the current discussion of deformation-induced nanocrystalline bulk materials, a thrust area is the reduction in grain-size of fcc-materials. For room-temperature deformation, the grain-size reduction of Al appears to be mainly limited because of dynamic recovery and recrystallization processes that can, however, be diminished upon deformation at cryogenic temperatures [36]. As an alternative to the reduction in grain-size, nanoscale Al crystallites can be induced upon crystallization of marginal glass formers. It has been demonstrated that upon annealing of, for example, melt-spun amorphous $Al_{88}Y_7Fe_5$ alloy nanocrystalline Al particles develop with size distributions that have their average typically in the range between 5 and 22 nm, depending on the annealing time and temperature [19, 37]. A size distribution of Al-nanocrystals in the size range between approximately 5 nm and 14 nm has been observed to develop during intense deformation of melt-spun amorphous $Al_{88}Y_7Fe_5$ ribbons [26]. Aside from a strong interest to identify the mechanism of deformation-induced crystallization reactions, earlier work on Fe-based glasses suggests that based on a combination of rolling and folding as well as annealing an increase in the nanocrystal density could be achieved as well as a reduction in the grain-size compared with ribbons that were annealed only [38].

In order to understand the response of amorphous metallic alloys to intense deformation, it is crucial to focus first on the amorphous phase in the as-prepared condition. It has become clear in recent years that for Al- or Fe-based glasses primary crystallization reactions can occur that are linked to heterogeneities or clusters retained during the quenching process [39]. In addition, computer simu-

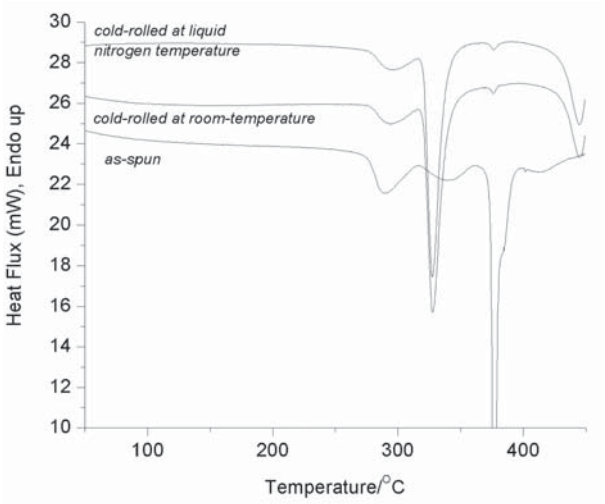

Fig. 5. Continuous heating DSC curves of as-spun amorphous $Al_{88}Y_7Fe_5$ ribbons and after rolling at room-temperature and at liquid nitrogen temperature.

lations suggest that the amorphous matrices can contain defects such as small volume elements with increased or diminished stress, density, or with a locally retained shear-stress [40,41]. Germane to primary crystallization reactions is a characteristic microstructural length scale, e.g. the average primary nanocrystal size which is of the order of a few nanometers. A key question is therefore, whether the deformation processes tend to homogenize the microstructures or if the level of heterogeneity is increased upon deformation. Experimental evidence for a cold-rolling induced dissolution of intermetallic $CuTi_2$ crystallites dispersed in an amorphous matrix was already found in [42]. Bending experiments with $Al_{85}Ni_{10}Ce_5$ ribbons demonstrated that nanocrystallites did not form in shear bands upon bending while for $Al_{90}Fe_5Gd_5$ ribbons nanocrystallites did develop [43]. Similar to bending, upon cold-rolling the formation of Al-nanocrystallites in $Al_{85}Ni_{10}Ce_5$ ribbons is not observed until strain levels in excess of -13 [44]. By comparison, for $Al_{88}Y_7Fe_5$ or $Al_{92}Sm_8$ ribbons, nanocrystallization occurs already at strain levels of -3 [26]. The $Al_{85}Ni_{10}Ce_5$ alloy differs not only from the $Al_{88}Y_7Fe_5$ and the $Al_{92}Sm_8$ alloys with respect to the deformation-response, but also in their thermally-induced crystallization behavior. The amorphous $Al_{85}Ni_{10}Ce_5$ sample does in contrast to the marginal glass formers $Al_{88}Y_7Fe_5$ or $Al_{92}Sm_8$ not reveal a primary crystallization reaction, but a crystallization of fcc-Al plus an unknown compound phase as crystallization products during the first crystallization reaction upon heating. Although the comparison between the marginal glass formers and amorphous ribbons such as $Al_{85}Ni_{10}Ce_5$ seems to suggest that retained heterogeneities are crucial to the rolling-induced crystallization reactions, more work is necessary to clarify, for example, whether the rolling process yields a growth of clusters or mediates a nucleation reaction in the amorphous matrix. The localization of the structural transformations to specific sites in the amorphous phase has been inferred also from molecular dynamic simulations. The simulation results indicate that shear transformation occurred at atomic sites that had the surrounding atoms organized in a geometric arrangement that had an orientation relation with respect to the external shear direction [45,46].

As an alternative explanation for the differences in the response to deformation, the formation of crystallites during deformation could result from adiabatic heating. Arguments in favor and against adiabatic heating as the reason for the deformation-induced crystallization reactions have been presented in [47], where it was concluded that an adiabatic heating effect could not explain the crystallization behavior observed during bending of $Al_{90}Fe_5Gd_5$ ribbons. In order to examine, if a deformation-induced, intrinsic heating effect in the ribbon could alter the thermal behavior of the ribbons after deformation, $Al_{88}Y_7Fe_5$ ribbons were cold-rolled at room-temperature and in a second rolling experiment with a liquid nitrogen flow that was directed into the roll gap during rolling. The melt-spun $Al_{88}Y_7Fe_5$ ribbons used for this experiment revealed an exothermic peak in the continuous heating DSC curve in the tempera-

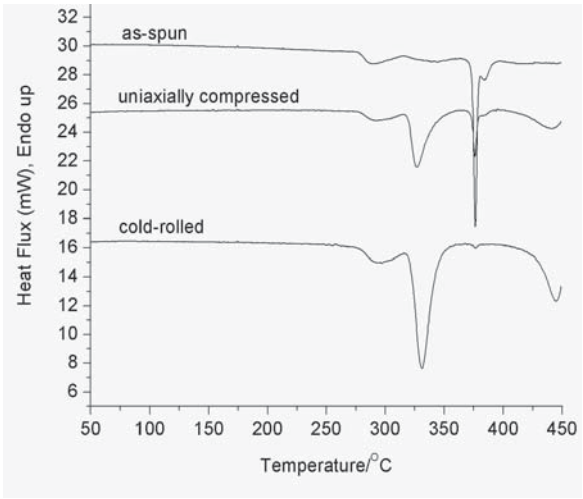

Fig. 6. Continuous heating DSC curves of as-spun amorphous $Al_{88}Y_7Fe_5$ ribbons and after rolling and uniaxial compression.

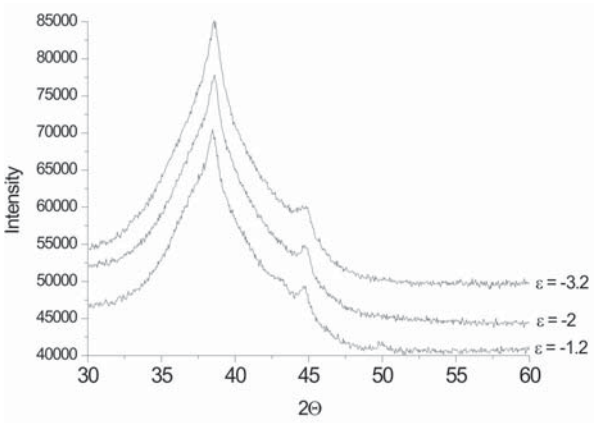

Fig. 7. XRD patterns of partially crystalline $Al_{88}Y_7Fe_5$ ribbons after rolling at different strain levels.

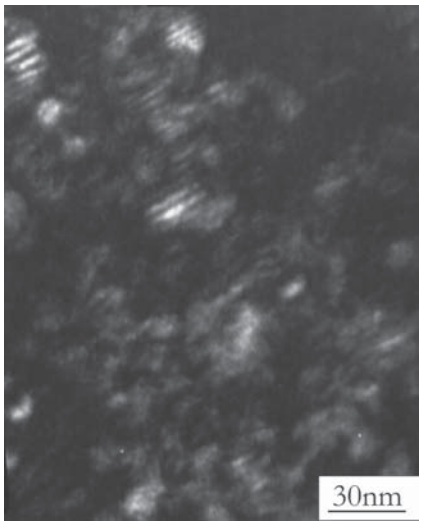

Fig. 8. TEM dark-field image of partially crystalline $Al_{88}Y_7Fe5$ ribbons at ε_{true} = -3.2.

ture range between the primary crystallization peak (onset temperature 278 °C) and the formation of the intermetallic phase (onset temperature 369 °C) as depicted in Fig. 5. The ribbon pieces used for the rolling at room-temperature and for the rolling in the liquid nitrogen flow were taken from the same master ribbon and were about 5 centimeters long, each. Both ribbons were rolled five times with the rollers touching each other. The DSC curves of the rolled ribbons that are depicted in Fig. 5 show the identical changes in the DSC curves, notably the strong increase of the transformation enthalpy for the second exothermic peak and the decrease for the third peak. The result indicates that the difference in the sample temperatures during deformation did not change the effect of the deformation on the post-deformation thermal behavior. This suggests that the mechanism causing the change in the thermal behavior of both ribbons is related to a mechanical rather than a heating effect. In an additional experiment, a melt-spun amorphous $Al_{88}Y_7Fe_5$ ribbon was divided into two halves. One half was compressed in a hand-press between two steel cylinders at a pressure of 300 MPa. The second half of the ribbon was cold-rolled, but not folded. Four pieces were again stacked on top of each other prior to the cold-rolling. The continuous heating DSC curves of the compressed and cold-rolled ribbons are depicted in Fig. 6. The primary crystallization peak is not affected at the given strain level, however, the second exothermic peak reveals changes for the rolled and compressed ribbons compared to the as-spun ribbon. Since the ribbons were in full contact with massive steel cylinders during the compression, a substantial heating effect during the compression can be ruled out. It appears, therefore, that the change in the thermal behavior of the compressed ribbons can not be thermally-induced.

In the discussion of crystallization processes it is important to identify, whether nucleation occurs homogeneously throughout the volume, or if nucleation is confined to specific nucleation sites. It is therefore helpful for the analysis of deformation-induced crystallization reactions to pay attention to the deformation mechanism of metallic glasses and to identify deformation-related nucleation sites. At temperatures below the glass transition temperature and for high stress levels, the deformation of amorphous materials is thought to be localized into shear bands while the regions surrounding the shear bands appear to be largely unaffected [43]. A key parameter is the free volume that appears to be enhanced in the shear bands. The average free volume per atom denotes the difference between the average volume per atom in the amorphous state and the Van der Waals volume of the atom [48]. It is the current understanding that the free volume increase in the shear-bands enhances the mobility in the shear-bands that in turn promotes nanocrystallization processes [49, 50]. This line of thought is undermined experimentally, since deformation-induced nanocrystals have been observed mainly at shear-bands so far.

The bending and cold-rolling experiments with Al-based amorphous alloys indicate a deformation-induced formation of nanocrystallites. The biggest

nanoparticles that have been observed after deformation of the $Al_{88}Y_7Fe_5$ alloy have a diameter of approximately 14 nm. While the growth of Al-nanocrystals during thermally-induced crystallization is limited due to solute partitioning and an overlap of diffusion-fields (soft impingement) [37], the size-limiting factors for deformation-induced crystallites have yet to be determined. In order to test, if the deformation process can induce a continued growth of pre-existing Al nanocrystallites, X-ray amorphous $Al_{88}Y_7Fe_5$ ribbons were annealed at 260 °C, i.e. 18 degrees below the onset of the primary crystallization reaction and afterwards cold-rolled to a strain of -3.2. The X-ray pattern of the annealed sample revealed the presence of Al. The X-ray patterns of the ribbons after annealing and after annealing and rolling that are depicted in Fig. 7 are very similar except for a slight broadening of the Al(200) peak. The TEM analysis of the sample that was rolled after annealing shows that there are Al-nanocrystals depicted in Fig. 8 that have a 'banded' microstructure. Since the TEM samples are in-plane samples, i.e. the electron beam direction is parallel to the sample normal, the bands observed in the Al-particles could reflect a Moiré effect. For rolled samples without annealing, a 'banded' image of the Al-nanocrystallites has never been observed. If the band structures are indeed due to a Moiré effect, then the rolling process would tend to align pre-existing or rolling-induced nanocrystals. This demonstrates again that the deformation processing offers opportunities for microstructure control that can not be achieved by thermal processing.

Parallel to the advances in the experimental findings, it is intriguing to consider the theoretical basis upon which the deformation-induced crystallization reactions can be rationalized. The key characteristic of deformation-induced transitions is the continuous energy input into the systems that must therefore be considered as open systems. Annealing-induced transformations, by contrast, are closed processes, where equilibrium thermodynamics is applicable [51]. Phase transformations are governed thermodynamically by the minimization of free energies. As described in detail in [52], driven system processing, e.g. deformation-processing, can no longer be rationalized in terms of the minimization of a thermodynamic potential, but must be addressed as a competition between the external forcing and thermal relaxation processes that evolves towards a dynamic steady-state. The rolling experiments with the $Al_{88}Y_7Fe_5$ ribbons demonstrate that the concepts that are applicable to thermal processing have to be modified for deformation processing. For example, the crystallites seem to develop mainly in the shear bands that, however, evolve during the deformation and an interaction between the crystallites and the shear band formation cannot be ruled out. By contrast, the nucleation sites for heterogeneous nucleation exist in most cases prior to the thermal processing.

4. CONCLUDING REMARKS

Two examples have been highlighted in this contribution that are based on a novel synthesis route for nanoscale materials that is promising particularly for structural materials. A continued rolling and folding process has been applied to multilayers of Al-based elemental foils as well as to Al-based amorphous ribbons. Despite the differences between multilayers of crystalline foils and amorphous ribbons, common underlying principles of deformation-induced structural transformation processes have been recognized. The transformations occur at structural heterogeneities of the parent phase. While the transformations in rolled multilayers occur at the interfaces between the dissimilar layers, the identification of the transformation sites in deformed ribbons is less obvious. At first glance, crystallization seems to be confined to bands in the amorphous matrix that are often identified as shear-bands. However, crystallites following deformation are also observed in the matrix, without any visible bands surrounding the crystallites. Studies based on Mössbauer spectroscopy of Fe-based, amorphous cold-rolled ribbons indicated that the defects that are introduced during the deformation were not localized, but distributed throughout the volume [53]. Certainly, the analysis of the crystallization sites in deformed amorphous alloys requires further attention. A second underlying principle is that the deformation-induced local transformation volumes are of the order of nanometers. For the multilayers, the local transformation volumes are the mixing zones across the interfaces that are limited to the nanometer level. The deformation-induced crystallites in the amorphous ribbons have diameters of less than approximately 15 nanometers. Since heating-effects have been ruled out, the mechanism of the deformation-induced growth of intermixed zones in multilayers or of nanocrystallites in amorphous matrices appears to be due to an athermally-enhanced mobility. A key characteristic of the deformation-induced transformations is that the transformation site density increases strongly. For the multilayers, the relative specific interface area can increase three orders of magnitude. For the ribbons,

the number of shear-bands or delocalized defects increases with deformation although the details are the subject of current research. The rapid increase of the transformation site density during the transformations sets the driven processing apart from thermal processing. In order to gauge the transformation behavior of driven systems, it is necessary to understand the dynamics of the evolution of the transformation sites. The rolling and folding experiments with the multilayers, but also with the amorphous ribbons demonstrate that the increase in the transformation site densities is governed mainly by the mechanical behavior of the multilayers or the amorphous phases.

A challenge for the application of nanoscale materials for structural applications is the availability of bulk samples. The cold-rolling process offers the prospect of a scale-up. Moreover, the laboratory rolling experiments have demonstrated that upon intense rolling the initial array of ribbons can be compacted into sheet material with thicknesses of more than 300 micrometers. In light of the outstanding success of thermal processing for the synthesis of structural materials, the application of driven system processing to heterogeneous microstructures represents a novel approach with an intricate link between mechanics and thermodynamics.

ACKNOWLEDGEMENT

The majority of the results presented in this article were obtained at the University of Wisconsin-Madison. The guidance and the enlightening discussions with Prof. J.H. Perepezko are gratefully acknowledged. At UW-Madison support for this work was received from the ARO (DAAD 19-01-1-0486). The continued interest of Dr. W. Mullins in deformation-induced structural phase transformations is gratefully acknowledged.

REFERENCES

[1] H.K. Hardy and T.J. Heal // *Progr. Met. Phys*. **5** (1954) 143.
[2] A. Kelly and R.B. Nicholson // *Progr. Met. Phys*. **10** (1963) 151.
[3] H. Gleiter // *Progr. Mat. Sci*. **33** (1988) 223.
[4] H. Gleiter, J. Weissmüller, O. Wollersheim and R. Würschum // *Acta Mater*. **49** (2001) 737.
[5] E.O. Hall *// Proc. Roy. Soc. B* **64** (1951) 747.
[6] N.J. Petch // *J. Iron Steel Inst*. **174** (1953) 25.
[7] J. Bevk, J.P. Harbison and J.L. Bell // *J. Appl. Phys*. **49** (1978) 6031.
[8] R.G. Hoagland, T.E. Mitchell, J.P. Hirth and H. Kung // *Phil. Mag. A* **82** (2002) 643.
[9] L. Schultz, In: *Amorphous metals and non-equilibrium processing*, ed. by M.Von Allmen (Les Editions de Physique: Les Ulis, 1984), p.135.
[10] M. Atzmon, J.D. Verhoeven, E.D. Gibson and W.L. Johnson // *Appl. Phys. Lett.* **45** (1984) 1052.
[11] P.H. Shingu, K.N. Ishihara, A. Otsuki and I. Daigo // *Mat. Sci. Engr.* **A304-306** (2001) 399.
[12] N. Tsuji, Y. Saito, S.H. Lee and Y. Minamino // *Adv. Engr. Mat.* **5** (2003) 338.
[13] F. Bordeaux, A.R. Yavari and P. Desré // *Mat. Sci. Engr*. **97** (1988) 129.
[14] A. Inoue, M. Yamamoto, H.M. Kimura and T. Masumoto // *J. Mat. Sci. Lett*. **6** (1987) 194.
[15] Y. He, G.J. Shiflet and S.J. Poon // *Science* **241** (1988) 1640.
[16] A.L. Greer // *Nature* **368** (1994) 688.
[17] S.J. Hong, P.J. Warren and B.S. Chun // *Mat. Sci. Engr.* **A304-306** (2001) 362.
[18] J.H. Perepezko, D.R. Allen and J.C. Foley, *U.S. Patent 6,261,386B1* (University of Wisconsin-Madison, Madison, WI 17 July 2001).
[19] J.H. Perepezko, R.J. Hebert, W.S. Tong, J. Hamann, H. Rösner and G. Wilde // *Mat. Trans.* **44** (2003) 1982.
[20] M. Gich, T. Gloriant, S. Surinach, A.L. Greer and M.D. Baro // *J. Non-Cryst. Solids* **289** (2001) 214.
[21] H. Chen, Y. He, G.J. Shiflet and S.J. Poon // *Nature* **367** (1994) 541.
[22] A. Ogura, R. Tarumi, M. Shimojo, K. Takashima and Y. Higo // *Appl. Phys. Lett.* **79** (2001) 1042.
[23] J.-J. Kim, Y. Choi, S. Suresh and A.S. Argon // *Science* **295** (2002) 654.
[24] J.H. Perepezko, R.J. Hebert and W.S. Tong // *Intermetallics* **10** (2002) 1079.
[25] W.H. Jiang, F.E. Pinkerton and M. Atzmon // *Scripta Mater*. **48** (2003) 1195.
[26] R.J. Hebert and J.H. Perepezko // *Mat. Sci. Engr. A*, in press, available online.
[27] D. Kuhlmann-Wilsdorf and M.S. Bednar // *Wear* **181-183** (1995) 922.
[28] R.J. Hebert and J.H. Perepezko // *Scripta Mater*. **50** (2004) 807.
[29] F. Bordeaux and A.R. Yavari // *Z. Metallkde*. **81** (1990) 130.

[30] S.L. Semiatin and H.R. Piehler // *Met. Trans*. **10A** (1979) 97.
[31] A.M. Russell, L.S. Chumbley and Y. Tian // *Adv. Engr. Mat*. **2** (2000) 11.
[32] X. Sauvage, L. Renaud, B. Deconihout, D. Blavette, D.H. Ping and K. Hono // *Acta Mater.* **49** (2001) 389.
[33] N. Mandal, S.K. Samanta, G. Bhattacharyya and C. Chakraborty // *J. Struct. Geology* **25** (2003) 1359.
[34] R.B. Schwarz // *Mater. Sci. Forum* **269-272** (1998) 665.
[35] A. C. Lund and C. A. Schuh // *Appl. Phys. Lett.* **82** (2003) 2017.
[36] Y. Wang, T. Jiao and E. Ma // *Mat. Trans.* **44** (2003) 1926.
[37] J.C. Foley, D.R. Allen and J.H. Perepezko // *Scripta Mat.* **35** (1996) 655.
[38] N.I. Noskova, N.F. Vil'danova, R.I. Tagirov, A.P. Potapov and A.A. Glazer // *Phys. Met. Metall* **67** (1989) 136.
[39] D.R. Allen, J.C. Foley and J.H. Perepezko // *Acta Mater.* **46** (1998) 431.
[40] K. Maeda and S. Takeuchi // *Phys. Stat. Sol. A* **49** (1978) 685.
[41] D. Srolovitz // *Phil. Mag. A* **44** (1981) 847.
[42] P.D. Askenazy, E.A. Kamenetzky, L.E. Tanner and W.L. Johnson // *J. Less Common Met.* **140** (1988) 149.
[43] H. Chen, Y. He, G.J. Shiflet and S.J. Poon // *Nature* **367** (1994) 541.
[44] R.J. Hebert, *Ph.D. Thesis*, University of Wisconsin-Madison, 2003.
[45] R. Tarumi, A. Ogura, M. Shimojo, K. Takashima and Y. Higo // *Mat. Res. Soc. Symp. Proc.* **634** (2001) B1.9.1.
[46] M.L. Falk and J. S. Langer // *MRS Bulletin* **25** (2000) 40.
[47] W.H. Jiang and M. Atzmon // *Acta Mater.* **51** (2003) 4095.
[49] M.H. Cohen and D. Turnbull // *J. Chem. Phys.* **31** (1959) 1164.
[50] H.J. Jin, F. Zhou, L.B. Wang and K. Lu // *Scripta Mater.* **44** (2001) 1083.
[51] J.-C. Claus and M. Von Heimendahl // *Z. Metallkde.* **74** (1983) 744.
[52] W.J. Boettinger and J.H. Perepezko, In: *Rapidly solidified alloys: processes, structures*, *properties, applications*, ed. by H.H. Liebermann (Marcel Dekker: New York, 1993), p. 17.
[53] G. Martin and P. Bellon // *Solid State Phys.* **50** (1997) 189.
[54] A. Gupta, S. Lal and R.P. Verma // *J. Appl. Phys.* **56** (1984) 3485.